Scattering of scalar waves by rotating black holes

Kostas Glampedakis[1] and Nils Andersson[2]
[1] *Department of Physics and Astronomy, Cardiff University, Cardiff CF2 3YB, United Kingdom*
[2] *Department of Mathematics, University of Southampton, Southampton SO17 1BJ, United Kingdom*

We study the scattering of massless scalar waves by a Kerr black hole by letting plane monochromatic waves impinge on the black hole. We calculate the relevant scattering phase-shifts using the Prüfer phase-function method, which is computationally efficient and reliable also for high frequencies and/or large values of the angular multipole indices (l,m). We use the obtained phase-shifts and the partial-wave approach to determine differential cross sections and deflection functions. Results for off-axis scattering (waves incident along directions misaligned with the black hole's rotation axis) are obtained for the first time. Inspection of the off-axis deflection functions reveals the same scattering phenomena as in Schwarzschild scattering. In particular, the cross sections are dominated by the glory effect and the forward (Coulomb) divergence due to the long-range nature of the gravitational field. In the rotating case the overall diffraction pattern is "frame-dragged" and as a result the glory maximum is not observed in the exact backward direction. We discuss the physical reason for this behaviour, and explain it in terms of the distinction between prograde and retrograde motion in the Kerr gravitational field. Finally, we also discuss the possible influence of the so-called superradiance effect on the scattered waves.

I. INTRODUCTION

Diffraction of scattered waves provides the explanation for many of Nature's most beautiful phenomena, such as rainbows and glories. It has long been recognized that these optical phenomena have analogies in many other branches of physics. They are of particular relevance to quantum physics, where plane wave "beams" are routinely used to probe the details of atoms, nuclei or molecules. Such experiments provide a deep understanding of the scatterer's physics and can be used as a powerful test of various theoretical models. The analogy can be extended also to gravitational physics and extreme astrophysical objects like black holes. In fact, black hole scattering has been the subject of a considerable amount of work carried out over the last 30 years (see [1] for an extensive review). In the case of astrophysical black holes it is unlikely that the various diffraction effects will ever be observed (although it is not entirely implausible that advances of current technology will eventually enable us to study interference effects in gravitationally lensed waves). However, it is nevertheless useful to have a detailed theoretical understanding of the scattering of waves from black holes. After all, a study of these problems provides a deeper insight into the physics of black holes as well as wave-propagation in curved spacetimes.

The benchmark problem for black-hole scattering is massless scalar waves impinging on a Schwarzshild black hole. This problem is well understood [2–8], and it is known that it provides a beautiful example of the glory effect. Handler and Matzner [9] have shown that the situation remains almost unchanged if, instead of scalar waves, one decides to "shoot" plane electromagnetic or gravitational waves towards the black hole. These authors have also considered on-axis scattering of gravitational waves in the case when the black hole is rotating [9]. Their results suggest that the scattering cross sections consist of essentially the same features as in the non-rotating case (there is a forward divergence due to the long-range nature of the gravitational field and a backward glory). In addition, they find some peculiar features that are, at the present time, not well understood. An explanation of these effects is complicated by the fact that they could be caused by several effects, the most important being the coupling between the black hole's spin and the spin/polarisation of the incident wave. Given that the available investigations have not been able to distinguish between these various effects, we feel that our current understanding is somewhat unsatisfactory. This feeling is enhanced by the fact that no results for the most realistic case, corresponding to off-axis incidence, have yet been obtained.

This paper provides an attempt to further our understanding of the scattering from rotating black holes. Our aim is to isolate those scattering effects that are due to the spin of the black hole. In order to do this, we focus our attention on the scattering of massless scalar waves. For this case, the infalling waves have neither spin nor polarisation and therefore one would expect the scattered wave to have a simpler character than in the physically more relevant case of gravitational waves. However, one can be quite certain that the features discussed in this paper will be present also in the case of gravitational waves. It is, after all, well known that the propagation of various fields in a given black hole geometry is described by very similar wave equations.

Although we will re-examine the case of axially incident waves, our main attention will be on the more interesting off-axis scattering cross sections. These cross sections turn out to be quite different from the ones available in the literature. Obviously, they have two degrees of freedom (corresponding to the two angles θ and φ in Boyer-Lindquist coordinates). In addition we will show that the cross sections are asymmetric with respect to the incidence direction. In particular, the glory moves away from the backward direction as a result of rotational frame dragging that provides a distinction between prograde and retrograde motion in the Kerr geometry.

We construct our differential cross sections using the well-known partial wave decomposition (for an introduction see [10]) — the standard approach in quantum scattering theory. That this method is equally useful in black-hole scattering is well established [1]. We should point out, however, that alternatives (such as the complex-angular momentum approach [11,12] and path-integral methods [7,13,14]) have also been succesfully applied to the black-hole case. In the partial wave picture all scattering information is contained in the radial wavefunction's phase shifts. The calculation of these phase-shifts must, apart from in exceptional cases like Coulomb scattering, be performed numerically. Various techniques have been developed for this task. Basically, one must be able to determine the phase-shifts accurately up to sufficiently large l partial waves that no interference effects are lost. This boils down to a need for many more multipoles to be studied as the frequency of the infalling wave is increased. In black-hole scattering several methods have been employed for the phase-shift calculation: Matzner and Ryan [2] numerically integrated the relevant radial wave equation (Teukolsky's equation). Since the desired solution is an oscillating function, this calculation becomes increasingly difficult (and time consuming) as the frequency is increased. Consequently, Matzner and Ryan restricted their study of electromagnetic and gravitational wave scattering to $\omega M \leq 0.75$ and $l \leq 10$. In order to avoid this difficulty, Handler and Matzner [9] combined a numerical solution in the region where the gravitational curvature potential varies rapidly, with an approximate WKB solution for relatively large values of the radial coordinate. This trick allowed them to perform calculations for $l \leq 20$ and $\omega M \leq 2.5$. Some years ago one of us used the phase-integral method [15,16] to derive an approximate formula for the phase-shifts in the context of Schwarzschild scattering [8]. This formula was shown to be reliable and efficient even for high frequencies and/or large l values (in [8] results for $\omega M = 10$ and $l \leq 200$ were presented). This means that the differential cross sections determined from the phase-integral phase-shifts were reliable also for rather high frequencies. Even though the phase-integral formula could be generalised to scattering by a Kerr black hole and therefore used for the purposes of the present study, we have chosen a different approach here. Our phase-shift determination is based on the so-called Prüfer method (well-known in quantum scattering theory [17,18] and, in general, in numerical treatments of Sturm-Liouville problems [19]) which, in a nutshell, involves transforming the original radial wavefunction to specific phase-functions and numerical integration of the resulting equations. In essence, this method is a close relative of the phase-amplitude method that was devised by one of us to study black-hole resonances [20].

The remainder of the paper is organised as follows. In Sections IIA and IIB the problem of scattering by a Kerr black hole is rigorously formulated. In Section IIC the important notion of the deflection function is discussed. Section III is devoted to our numerical results. First, in Section IIIA our numerical method for calculating phase-shifts is presented. In Section IIIB familiar Schwarzschild results are reproduced as a code validation. Sections IIIC and IIID contain entirely new information: Differential cross sections and deflection functions for on and off-axis scattering respectively. These are the main results of the paper. Furthermore, in Section IIIE we present numerical results concerning forward glories. The role of superradiance for scattering of monochromatic waves is discussed in Section IIIF. Our conclusions are briefly summarised in Section IV. Three appendices are devoted to technical details, which are included for completeness. In Appendix A we discuss the notion of "plane waves" in the presence of a gravitational field. In Appendix B the partial-wave decomposition of a plane wave in the Kerr background is determined, and finally in Appendix C we briefly describe the method we have used to calculate the spin-0 spheroidal harmonics and their eigenvalues. Throughout the paper we adopt geometrised units ($c = G = 1$).

II. SCATTERING FROM BLACK HOLES

A. Formulation of the problem

We consider a massless scalar field in the Kerr black-hole geometry. Then, first-order black-hole perturbation theory, basically the Teukolsky equation [21], applies. The scalar field satisfies the curved spacetime wave equation $\Box\Phi = 0$. Adopting standard Boyer-Lindquist coordinates we can always decompose the field as (since the spacetime is axially symmetric)

$$\Phi(r,\theta,\varphi,t) = \frac{1}{\sqrt{r^2+a^2}} \sum_{m=-\infty}^{+\infty} \phi_m(r,\theta,t) e^{im\varphi} \tag{1}$$

In scattering problems it is customary to consider monocromatic waves with given frequency ω. Therefore we can further write

$$\phi_m(r,\theta,t) = \sum_{l=|m|}^{+\infty} c_{lm} u_{lm}(r,\omega) S_{lm}^{a\omega}(\theta) e^{-i\omega t} \tag{2}$$

where c_{lm} is some expansion coefficient and $S_{lm}^{a\omega}(\theta)$ are the usual spin-0 spheroidal harmonics. These are normalised as

$$\int_0^\pi d\theta \sin\theta |S_{lm}^{a\omega}(\theta)|^2 = \frac{1}{2\pi} \tag{3}$$

Finally, the function $u_{lm}(r,\omega)$ is a solution of the radial Teukolsky equation:

$$\frac{d^2 u_{lm}}{dr_*^2} + \left[\frac{K^2 + (2am\omega - a^2\omega^2 - E_{lm})\Delta}{(r^2+a^2)^2} - \frac{dG}{dr_*} - G^2 \right] u_{lm} = 0 \tag{4}$$

where $K = (r^2+a^2)\omega - am$ and $G = r\Delta/(r^2+a^2)^2$. Furthermore, E_{lm} denotes the angular eigenvalue, cf. Appendix C. As usual, $\Delta = r^2 - 2Mr + a^2$ and the "tortoise" radial coordinate r_* is defined as (with $r_\pm$, the two solutions to $\Delta = 0$, denoting the event horizon and the inner Cauchy horizon of the black hole)

$$r_* = r + \frac{2Mr_+}{r_+ - r_-} \ln\left(\frac{r}{r_+} - 1\right) - \frac{2Mr_-}{r_+ - r_-} \ln\left(\frac{r}{r_-} - 1\right) + c \tag{5}$$

Usually, the arbitrary integration constant c is disregarded in this relation. However, in scattering problems it turns out to be useful to keep it, as we shall see later.

We are interested in a causal solution to (4) which describes waves that are purely "ingoing" at the black hole's horizon. This solution can be written

$$u_{lm}^{\text{in}} \sim \begin{cases} e^{-ikr_*} & \text{as } r \to r_+ \,, \\ A_{lm}^{\text{out}} e^{i\omega r_*} + A_{lm}^{\text{in}} e^{-i\omega r_*} & \text{as } r \to +\infty \,. \end{cases} \tag{6}$$

where $k = \omega - ma/2Mr_+ = \omega - m\omega_+$. In addition, we want to impose an "asymptotic scattering boundary condition". We want the total field at spatial infinity to be the sum of a plane wave plus an outgoing scattered wave. In other words, we should have

$$\Phi(r,\theta,\varphi) \sim \Phi_{\text{plane}} + \frac{1}{r} f(\theta,\varphi) e^{i\omega r_*} \quad \text{as} \quad r \to +\infty \tag{7}$$

where we have omitted the trivial time-dependence. All information regarding scattering is contained in the (complex-valued) scattering amplitude $f(\theta,\varphi)$. Note that, unlike in axially symmetric scattering the scattering amplitude will depend on both angles: θ and φ.

Up to this point, we have used the term "plane wave" quite loosely. In the presence of a long-range field such as the Kerr gravitational field (which falls off as $\sim 1/r$ at infinity) we cannot write a plane wave in the familiar flat space form. This problem has been discussed in several papers, see [23,24]. Remarkably, it turns out that in a black hole background the long-range character of the field is accounted for by a logarithmic phase-modification of the flat space plane-wave expression. In practice, the substitution $r \to r_*$ is made in the various exponentials. In order to make this paper as self-contained as possible, we discuss this point in some detail in Appendix A.

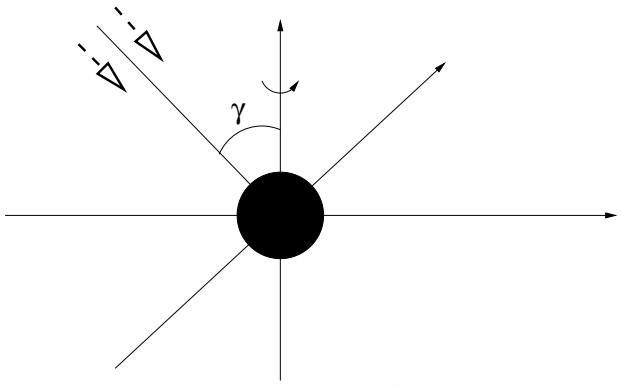

FIG. 1. A schematic illustration of the general scattering problem. A plane wave impinges on a rotating black hole making an angle γ with the rotation axis.

The asymptotic expression for a plane wave travelling along a direction making an angle γ with the black hole's spin axis, see Figure 1, is

$$\Phi_{\text{plane}} = e^{i\omega r_*(\sin\gamma\sin\theta\sin\varphi+\cos\gamma\cos\theta)} \tag{8}$$

where without any loss of generality we have assumed an amplitude of unity. We can decompose this plane wave in a way similar to (1) and (2);

$$\Phi_{\text{plane}} \approx \frac{1}{r}\sum_{m=-\infty}^{+\infty}\sum_{l=|m|}^{+\infty} c_{lm}^{(0)} u_{lm}^{(0)}(r,\omega) S_{lm}^{a\omega}(\theta) e^{im\varphi} \tag{9}$$

where $u_{lm}^{(0)}$ are asymptotic solutions of (4). For $r \to \infty$ we have (see Appendix B),

$$c_{lm}^{(0)} u_{lm}^{(0)}(r,\omega) \approx 2\pi S_{lm}^{a\omega}(\gamma)\left\{(-i)^{m+1}e^{i\omega r_*} + i^{m+1}(-1)^{l+m}e^{-i\omega r_*}\right\} \tag{10}$$

Similarly, the full field at infinity can be approximated as :

$$\Phi \approx \frac{1}{r}\sum_{m=-\infty}^{+\infty}\sum_{l=|m|}^{+\infty} c_{lm}(A_{lm}^{\text{in}}e^{-i\omega r_*} + A_{lm}^{\text{out}}e^{i\omega r_*}) S_{lm}^{a\omega}(\theta) e^{im\varphi} \tag{11}$$

By imposing the scattering condition (7), we can fix c_{lm} by demanding that the ingoing wave piece of $\Phi - \Phi_{\text{plane}}$ vanishes. After some straightforward manipulations we get for the scattering amplitude

$$f(\theta,\varphi) = \frac{2\pi}{i\omega}\sum_{m=-\infty}^{+\infty}\sum_{l=|m|}^{+\infty}(-i)^m S_{lm}^{a\omega}(\theta) S_{lm}^{a\omega}(\gamma) e^{im\varphi}\left[(-1)^{l+1}\frac{A_{lm}^{\text{out}}}{A_{lm}^{\text{in}}} - 1\right] \tag{12}$$

By defining the "scattering matrix element" $\mathcal{S}_{lm} = (-1)^{l+1}A_{lm}^{\text{out}}/A_{lm}^{\text{in}}$ we can equivalently write

$$\mathcal{S}_{lm} = e^{2i\delta_{lm}} \tag{13}$$

where we have introduced the phase-shift δ_{lm}. Thus we see that the phase-shifts δ_{lm} contain all relevant information regarding the scattered wave. It is worth emphasising that for non-axisymmetric scattering the phase-shifts will depend on both l and m. Also, the δ_{lm} are in general complex valued in order to account for absorption by the black hole. For later convenience, we also point out that the full field at infinity can be written

$$\Phi \sim \sin(\omega r_* + \delta_{lm} - \frac{l\pi}{2}) \quad \text{as } r_* \to \infty \tag{14}$$

In the case of on-axis incidence ($\gamma = 0$) the scattering amplitude simplifies considerably, and we get

$$f(\theta) = \frac{2\pi}{i\omega}\sum_{l=0}^{+\infty} S_{l0}^{a\omega}(\theta) S_{l0}^{a\omega}(0)\left[(-1)^{l+1}\frac{A_l^{\text{out}}}{A_l^{\text{in}}} - 1\right] \tag{15}$$

Here we see that the outcome is no longer dependent on m, which is natural given the axial symmetry of the problem. Furthermore, it is easy to see that we recover the familiar Schwarzschild expression [8] by setting $a = 0$.

The differential cross section (often simply called the cross section in this paper) is the most important "observable" in a scattering problem. It provides a measure of the extent to which the scattering target is "visible" from a certain viewing angle. As demonstrated in standard textbooks [10], the differential cross section follows immediately from the scattering amplitude

$$\frac{d\sigma}{d\Omega} = |f(\theta,\varphi)|^2 \ . \tag{16}$$

This cross section corresponds to "elastic" scattering only, that is, it describes the angular distribution of the waves escaping to infinity. We can similarly define an "absorption cross section" but we shall not be concerned with this issue here. Nevertheless, as we have already pointed out, black hole absorption has an effect on the phase-shifts that are used to compute the cross section (16).

The strategy then for a cross section calculation (for given black hole parameters and wave frequency) involves three steps: i) calculation of the phase-shifts δ_{lm}, (or, equivalently, of the asymptotic amplitudes $A_{lm}^{\text{out/in}}$), ii) calculation of the spheroidal harmonics $S_{lm}^{a\omega}(\theta)$, and finally iii) evaluation of the sums in (12) and/or (15) including a sufficiently large number of terms.

B. Approximating the scattering amplitude

In practice, the partial-wave sum calculation is problematic as it converges slowly. In fact, the sum is divergent for some angles. This is just an artifact due to the long-range nature of the gravitational field. No matter how far from the black hole a partial wave may travel, it will always "feel" the presence of the gravitational potential (that falls off as $1/r$). A similar behaviour is known to exist in Coulomb scattering. The divergence always occurs at the angle that specifies the incident wave's propagation direction. That this will be the case is easily seen from the identity

$$\sum_{l,m} S^{a\omega}_{lm}(\theta)e^{im\varphi}S^{a\omega}_{lm}(\gamma)e^{-im\pi/2} = \delta(\cos\theta - \cos\gamma)\delta(\varphi - \pi/2)\ , \tag{17}$$

which follows directly from the fact that the functions $S^{a\omega}_{lm}(\theta)e^{im\varphi}$ form an orthonormal set. The corresponding identity for on axis incidence is

$$\sum_{l} S^{a\omega}_{l0}(\theta)S^{a\omega}_{l0}(0) = \frac{1}{2\pi}\delta(\cos\theta - 1)\ . \tag{18}$$

From (17) we can deduce a peculiar feature: Although the scattering problem is physically insensitive to the actual φ of the incidence direction, the specific value $\varphi = \pi/2$ is imposed by the above relations. Of course, this has no physical relevance since the problem at hand is axially symmetric and we can, without any loss of generality, assume an incoming wave travelling along the direction $(\theta, \varphi) = (\gamma, \pi/2)$.

The fact that the Kerr gravitational field behaves asymptotically as a Newtonian one considerably simplifies the scattering amplitude calculation. We would expect that large l partial waves (strictly speaking when $l/\omega M \gg 1$) to essentially feel only the far-zone Newtonian field. In terms of the phase-shifts, we expect them to approach their Newtonian counterparts $\delta_{lm} \to \delta^N_l$ asymptotically. In order to secure this matching we add to our phase-shifts an "integration constant" $-2\omega M\ln(4\omega M) + \omega M$. In this way, we also get $r_* \to r_{\rm c}$, where $r_{\rm c} = r + 2M\ln(2\omega r)$ is the respective tortoise coordinate of the Coulomb/Newtonian problem. Such a manipulation is admissible given the arbitrariness in the choice of the constant c in (5).

In calculating the partial-wave sum for the scattering amplitude, it is convenient to split it into two terms:

$$f(\theta,\varphi) = f_D(\theta,\varphi) + f_N(\theta,\varphi) \tag{19}$$

Here, $f_D(\theta,\varphi)$ represents the part of the scattering amplitude that carries the information of the main diffraction effects, while $f_N(\theta,\varphi)$ denotes the Newtonian (Coulomb) amplitude. Explicitly we have

$$f_N(\theta,\varphi) = \frac{2\pi}{i\omega}\sum_{l,m} Y_{lm}(\theta)e^{im\varphi}Y_{lm}(\gamma)(-i)^m\left[e^{2i\delta^N_l} - 1\right] \tag{20}$$

where we have deliberately "forgotten" the spherical symmetry of the Newtonian potential (which would had allowed us to write f_N as a function of θ only, and thus in terms of a sum over l). However, the Newtonian phase-shifts δ^N_l are still given by the well-known expression [1],

$$e^{2i\delta^N_l} = \frac{\Gamma(l+1-2i\omega M)}{\Gamma(l+1+2i\omega M)} \tag{21}$$

After simple manipulations we get

$$f_N(\xi) = \frac{1}{2i\omega}\sum_{l=0}^{+\infty}(2l+1)P_l(\cos\xi)(e^{2i\delta^N_l} - 1) \tag{22}$$

where $\cos\xi = \cos\theta\cos\gamma + \sin\theta\sin\gamma\sin\varphi$. The sum in (22) is known in closed form [1];

$$f_N(\xi) = M\frac{\Gamma(1-2i\omega M)}{\Gamma(1+2i\omega M)}\left[\sin\frac{\xi}{2}\right]^{-2+4i\omega M} \tag{23}$$

From this we can see that $f_N(\theta,\varphi)$ diverges in the $\xi = 0$ direction.

Let us now focus on the "diffraction" amplitude $f_D(\theta,\varphi)$. It has the form

$$f_D(\theta,\varphi)=\frac{2\pi}{i\omega}\sum_{m=-\infty}^{+\infty}\sum_{l=|m|}^{+\infty}(-i)^m e^{im\varphi}\left\{S^{a\omega}_{lm}(\theta)S^{a\omega}_{lm}(\gamma)(e^{2i\delta_{lm}}-1)-Y_{lm}(\theta)Y_{lm}(\gamma)(e^{2i\delta^N_l}-1)\right\} \tag{24}$$

The corresponding on-axis expression is,

$$f_D(\theta)=\frac{1}{2i\omega}\sum_{l=0}^{+\infty}\left\{4\pi S^{a\omega}_{l0}(\theta)S^{a\omega}_{l0}(0)(e^{2i\delta_l}-1)-(2l+1)P_l(\cos\theta)(e^{2i\delta^N_l}-1)\right\} \tag{25}$$

One would expect the sums in (24) and (25) to converge. This follows from the fact that for $l/\omega M\to\infty$ we have $\delta_{lm}\to\delta^N_l$ and $S^{a\omega}_{lm}(\theta)e^{im\varphi}\to Y_{lm}(\theta,\varphi)$ [9]. We introduce a negligible error by truncating the sums at a large value $l_{\rm max}$ (say). In practice, $l_{\rm max}$ need not be very large. We find that a value $\sim 30-50$ for $\omega M\lesssim 2$ typically suffices. Since each partial wave can be labelled by an impact parameter $b(l)$ (see Section IID), the criterion for $l_{\rm max}$ to be a "good" choice, is that $b(l_{\rm max})\gg b_{\rm c}$, where $b_{\rm c}$ is the (largest) critical impact parameter associated with an unstable photon orbit in the Kerr geometry.

The truncation of the partial-wave sums will introduce interference oscillations in the final cross sections (roughly with a wavelength $2\pi/l_{\rm max}$ [9]). These unphysical oscillations can be eliminated by following the approach of Handler and Matzner [9]. For a chosen $l_{\rm max}$ we add a constant β to all the phase-shifts in (24) and (25). This constant is chosen such that $\delta_{l_{\rm max},m}+\beta=\delta^N_l$. This means that the resulting cross section is effectively smoothed.

C. Deflection functions

It is well-know that the so-called deflection function is of prime importance in scattering problems. It arises in the semiclassical description of scattering, as discussed in the pioneering work of Ford and Wheeler [25]. Although these authors considered scattering in the context of quantum theory, their formalism is readily extended to the black-hole case. In the semiclassical paradigm, the phase-shifts are approximated by a one-turning point WKB formula (typically useful for l much larger than unity).

In a problem which has only one classical turning point, the deflection function is defined as

$$\Theta(l)=2\frac{d\delta^{\rm WKB}}{dl} \tag{26}$$

where l is assumed to take on continous real values. As a convention, the deflection function is negative for attractive potentials. The right-hand side of this equation resembles the expression for the deflection angle of classical motion in the given potential, provided that we define the following effective impact parameter b for the wave motion [10]

$$b=\frac{l+1/2}{\omega} \tag{27}$$

The black-hole effective potential has two turning points, but for $l/\omega M\to\infty$ the scattering is mainly due to the outer turning point and one can derive a one turning point WKB approximation for the phase shifts. For a Schwarzschild black hole this expression is [8]

$$\delta^{\rm WKB}_l=\int_t^{+\infty}\left[Q_{\rm s}-\left(1-\frac{2M}{r}\right)^{-1}\omega\right]dr-\omega t_*+(2l+1)\frac{\pi}{4} \tag{28}$$

where

$$Q^2_{\rm s}=\left(1-\frac{2M}{r}\right)^{-2}\left[\omega^2-\left(1-\frac{2M}{r}\right)\frac{l(l+1)}{r^2}+\frac{M^2}{r^4}\right] \tag{29}$$

Here t_* denote the value of the tortoise coordinate corresponding to the (outer) turning point t. We now define the deflection function as

$$\Theta(l)=2Re\left[\frac{d\delta_l}{dl}\right] \tag{30}$$

where only the real part of the phase shift is considered, as the whole discussion is relevant for elastic scattering only. Using (28), we find that the real scattering angle is

$$\Theta(l) = \pi - 2\left(\frac{l+1/2}{\omega}\right)\int_t^{+\infty}\frac{dr}{r^2}\left[1-\left(1-\frac{2M}{r}\right)\left(\frac{l+1/2}{\omega r}\right)^2+\mathcal{O}(M^2/r^2)\right]^{-1/2} \tag{31}$$

This WKB result should be compared to the deflection angle for a null geodesic in the Schwarzschild geometry, which is given by

$$\Theta_c(b) = \pi - 2b\int_t^{+\infty}\frac{dr}{r^2}\left[1-\left(1-\frac{2M}{r}\right)\frac{b^2}{r^2}\right]^{-1/2} \tag{32}$$

where $b = L_z/E$ is the orbit's impact parameter (L_z and E denote, respectively, the orbital angular momentum component along the black hole's spin axis and the orbital energy) and t is the (classical) turning point. In writing down these expressions we have chosen the signs in such a way that the deflection angle is negative for attractive potentials. Clearly, it is possible to "match" the deflection function (30) with the classical deflection angle, albeit only at large distances. Since the effective impact parameter will be given by (27), it is clear that in (31) the integral will be over large r only.

Owing to its clear geometrical meaning the deflection function is an exceptionally useful tool in scattering theory. It can be used to define diffraction phenomena like glories, rainbows etc. [25]. For example, in axisymmetric scattering backward glories are present if the deflection function takes on any of the values $\Theta = -n\pi$, where n a positive odd integer.

It seems natural to try and define deflection functions for Kerr scattering as well. In general, we anticipate the need for two deflection functions $\Theta(l,m)$ and $\Phi(l,m)$ (with only the first being relevant for the special case of on-axis scattering). The WKB phase-shift formula becomes in the Kerr case:

$$\delta_{lm}^{\rm WKB} = \int_t^{+\infty}\left[Q_{\rm k}-\left(\frac{r^2+a^2}{\Delta}\right)\omega\right]dr - \omega t_* + (2l+1)\frac{\pi}{4} \tag{33}$$

where

$$Q_{\rm k}^2 = \frac{1}{\Delta^2}\left[K^2 - \lambda\Delta + M^2 - a^2\right] \tag{34}$$

where $\lambda = E_{lm} + a^2\omega^2 - 2am\omega$.

The next step is to derive the deflection angles for null geodesics approaching a Kerr black hole from infinity. Such orbits are studied in detail in [26]. From the results in [26] it is clear that it is not easy to write down a general expression for the deflection angle in the Kerr case. But we can obtain useful results in two particular cases.

We begin by considering a null ray with $L_z = 0$ (which would correspond to an axially incident partial wave). For such an orbit we find that the deflection angle $\Theta_{\rm c}$ obeys the following relation

$$\int_\pi^{\Theta_{\rm c}(\eta)} d\theta\left[1+\frac{a^2}{\eta^2}\cos^2\theta\right]^{-1/2} = -2\eta\int_t^{+\infty}\frac{dr}{r^2}\left[1-\frac{\eta^2}{r^2}\left(1-\frac{2M}{r}+\frac{a^2}{r^2}\right)+\frac{a^2}{r^2}+\frac{2a^2M}{r^3}\right]^{-1/2} \tag{35}$$

where $\eta = C^{1/2}/E$, with C denoting the orbit's Carter constant. This expression is valid provided the ray's θ-coordinate varies monotonically during scattering. This should be true in the cases we are interested in, at least for large impact parameters such that $\eta \gg M$. The ray will also be deflected in the φ-direction but this deflection carries no information regarding plane-wave scattering due to the axisymmetry of the problem.

We next consider a null ray travelling in the black hole's equatorial plane. This situation will be particularly relevant for a plane wave incident along $\gamma = \pi/2$. The net azimuthal deflection $\Phi_{\rm c}(b)$ for an impact parameter $b = L_{\rm z}/E$ is

$$\Phi_{\rm c}(b) = \pi - 2b\int_t^{+\infty}\frac{dr}{r}\left[1-\frac{a^2}{\Delta}+\frac{2aMr}{\Delta b}\right]\left[r^2+a^2+\frac{2a^2M}{r}-b^2\left(1-\frac{2M}{r}\right)-\frac{4aMb}{r}\right]^{-1/2} \tag{36}$$

Working to the same accuracy in terms of M/r as in the Schwarzschild case, we can match (35) and (36) to $\partial\delta_{lm}/\partial l$. This matching becomes possible if we use the following approximate expression for the eigenvalue E_{lm} [9]

$$E_{lm} \approx l(l+1) - \frac{1}{2}a^2\omega^2 + \mathcal{O}(\frac{a^3\omega^3}{l}) \tag{37}$$

As in the Schwarzschild case we assume that the effective impact parameter is given by (27). Although there is no occurrence of the multipole m in the above expressions, one can argue (from the symmetry of the various spheroidal

harmonics, which is similar to that of the spherical harmonic of the same (l, m)) that the classical angles (35) and (36) are related to partial waves with $m = 0$ and incidence $\gamma = 0$ and partial waves with $m = \pm l$ and incidence $\gamma = \pi/2$, respectively. Hence, we define the latitudinal deflection function

$$\Theta(l) = 2Re\left[\frac{\partial \delta_{lm}}{\partial l}(m = 0)\right] \tag{38}$$

and the azimuthal ("equatorial") deflection function

$$\Phi(l) = 2Re\left[\frac{\partial \delta_{lm}}{\partial l}(m = \pm l)\right] \tag{39}$$

III. NUMERICAL RESULTS

A. Phase-shifts calculation via the Prüfer transformation

In order to determine the required scattering phase-shifts we have used a slightly modified version of the simple Prüfer transformation, well-known from the numerical analysis of Sturm-Liouville problems [19]. The method is best illustrated by a standard second order ordinary differential equation:

$$\frac{d^2\psi}{dx^2} + U(x)\psi = 0 \tag{40}$$

where we can think of x as being a radial coordinate, spanning the entire real axis, and U an effective potential (in our problem corresponding to a single potential barrier) with asymptotic behaviour

$$U(x) \sim \begin{cases} k^2 & \text{as } x \to -\infty \ , \\ \omega^2 & \text{as } x \to +\infty \ . \end{cases} \tag{41}$$

with ω and k real constants. (The black hole problem we are interested in does, of course, have exactly this nature.) The solution of (40) will take the form of oscillating exponentials for $x \to \pm\infty$. Let us assume that we are looking for a solution to (40) with purely "ingoing" behaviour at the "left" boundary ($x \to -\infty$) and mixed ingoing/outgoing behaviour as $x \to +\infty$:

$$\psi \sim \begin{cases} e^{-ikx} & \text{as } x \to -\infty \ , \\ B\sin[\omega x + \zeta] & \text{as } x \to +\infty \ . \end{cases} \tag{42}$$

where ζ and B are complex constants. We can then write the exact solution of (40) in the form

$$\psi(x) = e^{\int P(x)dx} \tag{43}$$

The function $P(x)$ is the logarithmic derivative of $\psi(x)$ (a prime denotes derivative with respect to x)

$$\frac{\psi'}{\psi} = P \tag{44}$$

which obeys the boundary condition $P(x) \to -ik$ for $x \to -\infty$.

Similarly, we can express the function ψ and its derivative via a Prüfer transformation;

$$\psi(x) = B\sin[\omega x + \tilde{P}(x)] \tag{45}$$

$$\psi'(x) = B\omega\cos[\omega x + \tilde{P}(x)] \tag{46}$$

with $\tilde{P}(x)$ a Prüfer phase function which has ζ as its limiting value for $x \to +\infty$. Direct substitution in (40) yields the equations

$$\frac{dP}{dx} + P^2 + U(x) = 0 \tag{47}$$

$$\frac{d\tilde{P}}{dx} + \left[\omega - \frac{U(x)}{\omega}\right] \sin^2(\tilde{P} + \omega x) = 0 \tag{48}$$

The idea is to numerically integrate (47) and (48) instead of the original equation (40). The motivation for this is that, while the original solution may be rapidly oscillating, the phase-functions P and $\tilde{P}$ are expected to be slowly varying functions of x.

We expect this integration scheme to be considerably more stable, especially for high frequencies, than any direct approach to (40). Moreover, eqs. (47) and (48) are well behaved also at the classical turning points and are well suited for barrier penetration problems. However, if we want to ensure that the phase-functions are smooth and non-oscillatory we must account for the so-called Stokes phenomenon — the switching on of small exponentials in the solution to an equation of form (40). To do this we simply shift from studying $P(x)$ (which is calculated from $x = -\infty$ up to the relevant matching point $x_{\rm m}$) to $\tilde{P}(x)$ (which is calculated outwards to $x = +\infty$). In practice, the calculation is stable and reliable if the switch is done in the vicinity of the maximum of the black-hole potential barrier (the essential key is to not use one single representation of the solution through the entire potential barrier). The two phase functions are easily connected by

$$\tilde{P}(x) = -\omega x + \frac{1}{2i} \ln\left[\frac{iP - \omega}{iP + \omega}\right] \tag{49}$$

Finally, the desired phase-shift can be easily extracted as $\delta_{lm} = \zeta + l\pi/2$.

A major advantage of the adopted method is that it permits direct calculation of the partial derivatives $\partial\delta_{lm}/\partial l$ and $\partial\delta_{lm}/\partial m$, which are required for the evaluation of the deflection functions from Section IID. The equations for the l, m-derivatives of P and $\tilde{P}$ are simply found by differentiation of (47) and (48). For the case of scattering by a Kerr black hole, calculation of δ_{lm} and its derivatives with respect to l, m requires knowledge of the angular eigenvalue E_{lm} (see Appendix C) and its l, m-derivatives. We have used an approximate formula which is a polynomial expansion in $a\omega$ (formula 21.7.5 of [28]). This expression (and its derivatives) is well behaved for all integer values of l and m. However, it is divergent for the half-integer values $l = 1/2, 3/2, 5/2$. Hence, the numerical calculation of the deflection function will fail at these points, and will be generally ill-behaved in their neighbourhood. For the full cross section calculation, we additionally need to calculate the spin-0 spheroidal harmonics $S^{a\omega}_{lm}(\theta)$. This calculation is discussed in detail in Appendix C.

B. Schwarzschild results

In this section we reproduce phase-shifts and cross sections for Schwarzschild scattering. The purpose of this exercise is to validate, and demonstrate the reliability of, our numerical methods. We compare our numerical integration results to ones obtained using the phase-integral method [8].

As a first crucial test we compare, in Fig. 2, the first 100 phase-shifts for $\omega M = 1$. Because of the multi-valued nature of the phase-shifts we always plot the quantity $\mathcal{S}_l = e^{2i\delta_l}$. As is evident from Fig. 2, the agreement between our numerical phase-shifts and the phase-integral ones is excellent. This is equally true for a all frequencies examined (up to $\omega M = 10$). It should be noted that $\mathcal{S}_l$ is essentially zero (δ_l has a positive imaginary part) for those values of l for which absorption by the black hole is important. That this is the case for the lowest multipoles is clear from Fig. 2. As l increases δ_l becomes almost real and as a consequence $\mathcal{S}_l$ is almost purely oscillating.

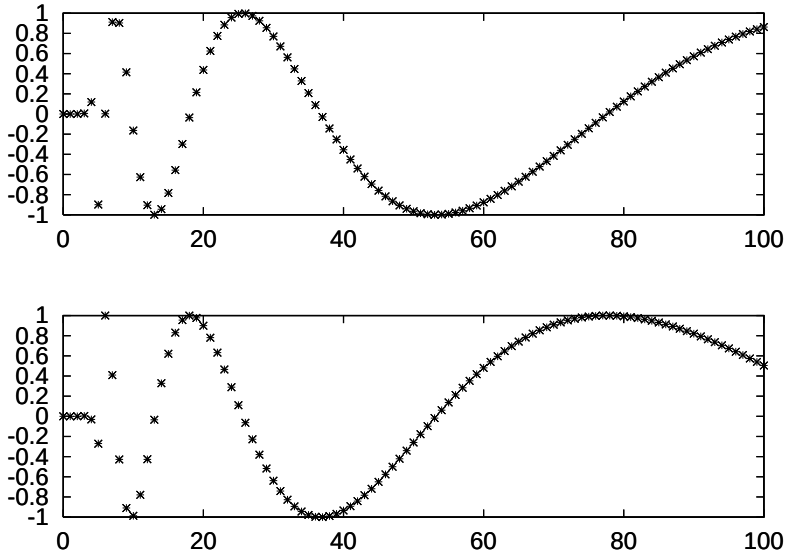

FIG. 2. Comparison of numerical phase-shifts for a Schwarzschild black hole (cross), against phase-integral data (plus). We show the real (upper frame) and imaginary (lower frame) parts of the scattering matrix element $\mathcal{S}_l = e^{2i\delta_l}$ as functions of l. The agreement between the two methods is clearly excellent.

In Fig. 3 we present an $\omega M = 10$ cross section generated from our numerical phase-shifts. For this particular calculation we have used $l_{\max} = 200$. The resulting cross section matches the one constructed using approximate phase-integral phase shifts perfectly. This demonstrates the efficiency of our approach in the high frequency regime, and it is clear that our study of Kerr scattering will not be limited by the lack of reliable phase shifts. However, the Kerr study is nevertheless limited in the sense that ω cannot be taken to be arbitrarily large. This restriction is imposed by the calculation of the spheroidal harmonics (Appendix C). However, it is important to emphasize that the most interesting frequency range, as far as diffraction phenomena is concerned, is $\omega M \sim 2$ [8]. Thus, we expect that our investigation should be able to reliable unveil all relevant rotational effects in the scattering problem.

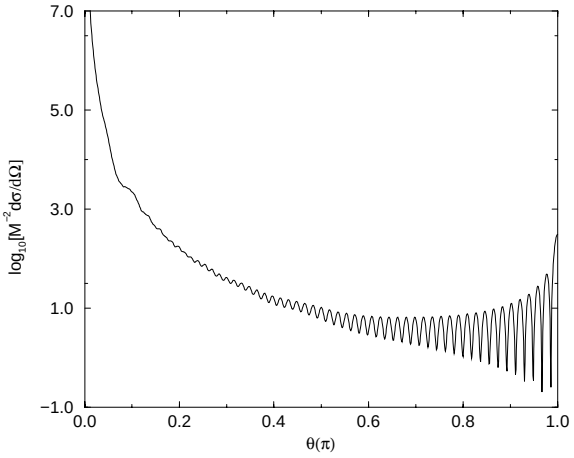

FIG. 3. Differential cross section for scattering of a wave with relatively high frequency, $\omega M = 10$, from a Schwarzschild black hole, based on the the first 200 partial wave phase-shifts. The backward glory oscillations are prominent.

We also find that the numerical values for $d\delta_l/dl$ are in good agreement with the respective phase-integral results. As a final remark we should emphasize that the numerical approach adopted in this work is very efficient from a computational point of view.

C. On-axis Kerr scattering

Having confirmed the reliability of our numerical results we now turn to the study of scattering of axially incident scalar waves by a Kerr black hole, cf. Fig. 4. In principle, we would expect the corresponding cross sections to be qualitatively similar to the Schwarzschild ones. The main reason for this is the inability of axially impinging partial waves to distinguish between prograde and retrograde orbits. However, examination of the orbital equations [26] reveals that the critical impact parameter (associated with the unstable photon orbit) decrease sligthly from the value $3\sqrt{3}M$ as the black hole spins up. For example, for a=0.99M we have $b_c = 4.74M$.

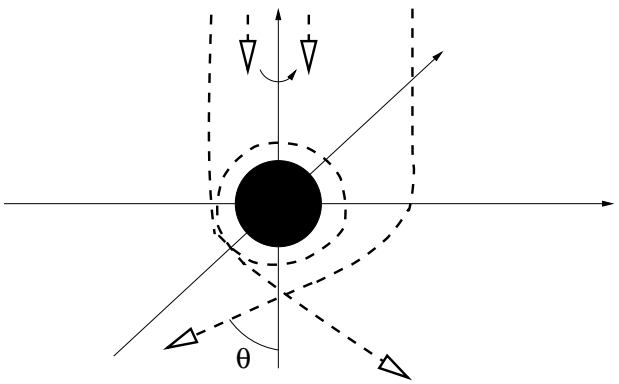

FIG. 4. A schematic drawing illustrating the case of on-axis scattering from a rotating black hole. Because of the axial symmetry of the problem, the scattering results are qualitatively similar to those for a Schwarzschild black hole. Two rays, which emerge having been scattered by the same angle θ are indicated.

Indeed, Fig. 5 confirms our expectations. The data in the figure corresponds to a black hole with spin $a = 0.99M$ and a wave frequency of $\omega M = 2$. For purposes of comparison, we also show the corresponding Schwarzschild cross section. The two cross sections are very similar. In particular, they are both dominated by the backward glory. It is well-known [1,7] that for Schwarzschild scattering the glory effect can be described in terms of Bessel functions. It has been shown that for $\theta \approx \pi$ the glory cross section can be approximated by

$$\frac{d\sigma}{d\Omega}(\theta)|_{\rm glory} \propto J_0^2[\omega b_{\rm c} \sin\theta] \tag{50}$$

A similar result holds for the backward glory in the case of on-axis Kerr scattering. Since b_c gets smaller, one would expect the zeros of the Bessel function (the diffraction minima) to move further away from $\theta = \pi$ as a increases. This effect is indicated by the data in Fig. 5.

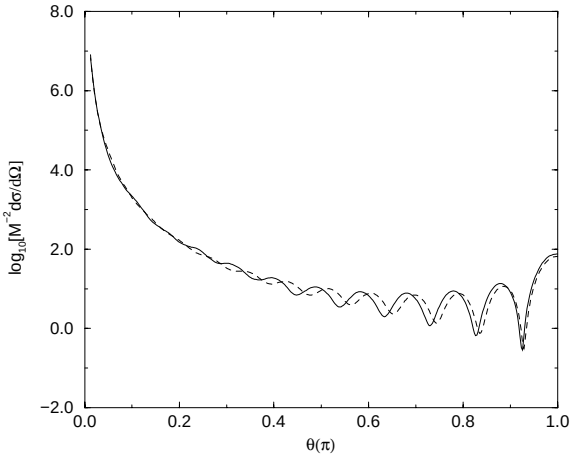

FIG. 5. Differential cross section for on-axis scattering from a Kerr black hole (solid line). The black hole's spin is $a = 0.99M$ and $\omega M = 2$. The graph is based on data for $l_{max} = 30$. The dashed line represents the corresponding Schwarzschild cross section.

The above conclusions are further supported by the results for the deflection function (38), as shown in Fig. 6. Because of the inaccuracies inherent in our method of calculating the deflection function for the lowest l-multipoles, see the discussion in Section IIIA, we do not show results for this regime. This is, however, irrelevant as the corresponding partial waves are expected to be more or less completely absorbed by the black hole.

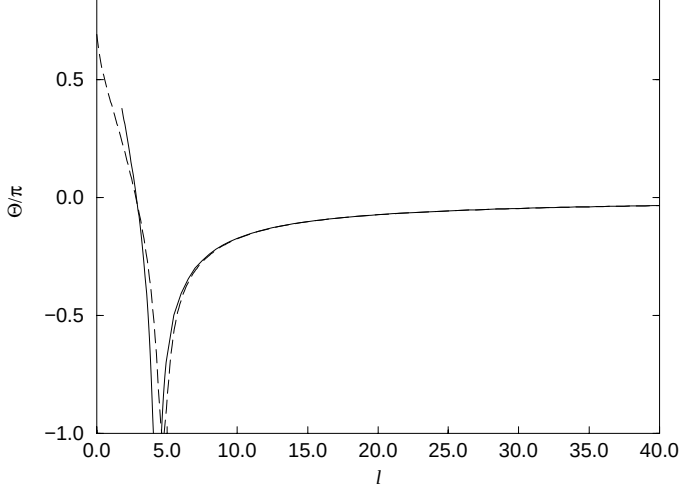

FIG. 6. Deflection function (in units of π) for on-axis scattering from a Kerr black hole. The black hole spin is $a = 0.99M$ and $\omega M = 1$. The dashed curve is the corresponding Schwarzschild deflection function. This figure confirms the behaviour expected from the geometric optics considerations, namely, the slight decrease of the critical impact parameter with increasing a.

D. Off-axis Kerr scattering

The conclusions of our study of on-axis scattering are perhaps not very exciting. Once the Schwarzschild case is understood, the on-axis results for Kerr come as no surprise. This is, however, not the case for off-axis scattering, cf. Fig. 7, where several new features appear.

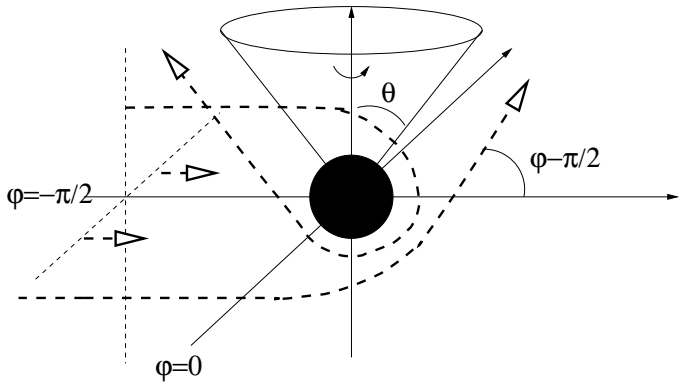

FIG. 7. A schematic drawing illustrating off-axis scattering from a rotating black hole. We show (as thick dashed lines) two "rays", one of which corresponds to motion in the black hole's equatorial plane.

Our study of the off-axis case provides the first results for non-axisymmetric wave scattering in black hole physics. Since this problem has not been discussed in great detail previously, it is worthwhile asking whether we can make any predictions before turning to the numerical calculations. Two effects ought to be relevant: First of all, the partial waves now have orbital angular momentum which couples to the black hole's spin. As a result the partial waves can be divided into prograde ($m > 0$) and retrograde ($m < 0$) ones. We expect prograde waves to be able to approach closer to the horizon than retrograde ones. In the geometric optics limit, prograde and retrograde rays tend to have increasingly different critical impact parameters as $a \to M$. As a second feature, we expect to find that large l partial waves will effectively feel only the spherically symmetric (Newtonian) gravitational potential. In other words, partial waves with the same (large) l and different values of m will approximately acquire the same phase-shift.

Our numerical results essentially confirm these expectations, as is clear from the phase-shifts (calculated for $a = 0.9M$ and $\omega M = 1$) shown in Fig. 8. As above, we have graphed the single-valued quantity $\mathcal{S}_{lm} = e^{2i\delta_{lm}}$ as a function of l. For each value of l we have included all the phase-shifts for $-l \leq m \leq +l$. The solid (dashed) line corresponds to $m = +l$ ($m = -l$) and the intermediate values of m lead to results in between these two extremes. For $l \gg 1$,

partial waves with different values of m have almost the same phase-shift. This is easy to deduce from the fact that the two curves approach each other as l increases. On the other hand, for the first ten or so partial waves we get very different results for the various values of m. In particular, we see that phase-shifts with $m > 0$ become almost real (that is, $|\mathcal{S}_{lm}|$ becomes non-zero) for a smaller l-value as compared to the $m < 0$ ones. As anticipated, this is due to the different critical impact parameters associated with prograde/retrograde motion, and the fact that a larger number of prograde partial waves are absorbed by the black hole.

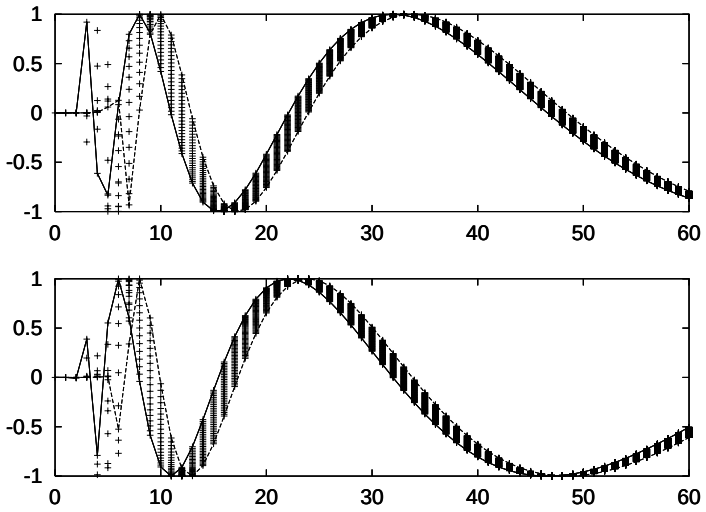

FIG. 8. Off-axis phase-shifts for $\omega M = 1$ and $a = 0.9M$. We illustrate the real (upper panel) and imaginary (lower panel) parts of $\mathcal{S}_{lm} = e^{2i\delta_{lm}}$ as functions of l, including all permissible values of m. The two curves correspond to $m = l$ (solid line) and $m = -l$ (dashed line).

We now turn to the cross section results for the off-axis case. We have considered a plane wave incident along the direction $\gamma = \varphi = \pi/2$. Even though our formalism allows incidence from any direction we have focussed on this case, which is illustrated in Fig. 7. The motivation for this is that there will then be partial waves (specifically the ones with $m = \pm l$) that are mainly travelling in the black hole's equatorial plane. These partial waves are important because one would expect them to experience the strongest rotational effects. Besides, we can obtain an understanding of these waves by studying equatorial null geodesics in the geometric optics limit. Equatorial null rays are much easier to describe than nonequatorial ones. This proves valuable in attempts to "decipher" the off-axis cross sections, and the obtained conclusions provide an understanding also of the general case.

In Fig. 9 we present a series of cross sections as functions of φ for the specific values $\theta = \pi/8, \pi/4, 3\pi/8, \pi/2$. These results correspond to viewing the scattered wave on the circumference of cones (like that shown in Fig. 7) with increasing opening angles. Two different frequencies $\omega M = 1$ and $\omega M = 2$ have been considered for a black hole with spin $a = 0.9M$. A first general remark concerns the asymmetry of the cross sections with respect to the incidence direction (note, however, that as a consequence of our particular choice of incidence direction there is still a reflection symmetry with respect to the equator). We can also easily distinguish the Coulomb forward divergence in the direction $\theta = \varphi = \pi/2$. Another obvious feature in Fig. 9 is the markedly different appearance of the cross section for different values of θ. As we move away from the equatorial plane the cross sections becomes increasingly featureless. This behaviour is artificial in the sense that as θ decreases, we effectively observe along a smaller circumference. At $\theta = 0$ this circumference degenerates into a point, cf. Fig. 7.

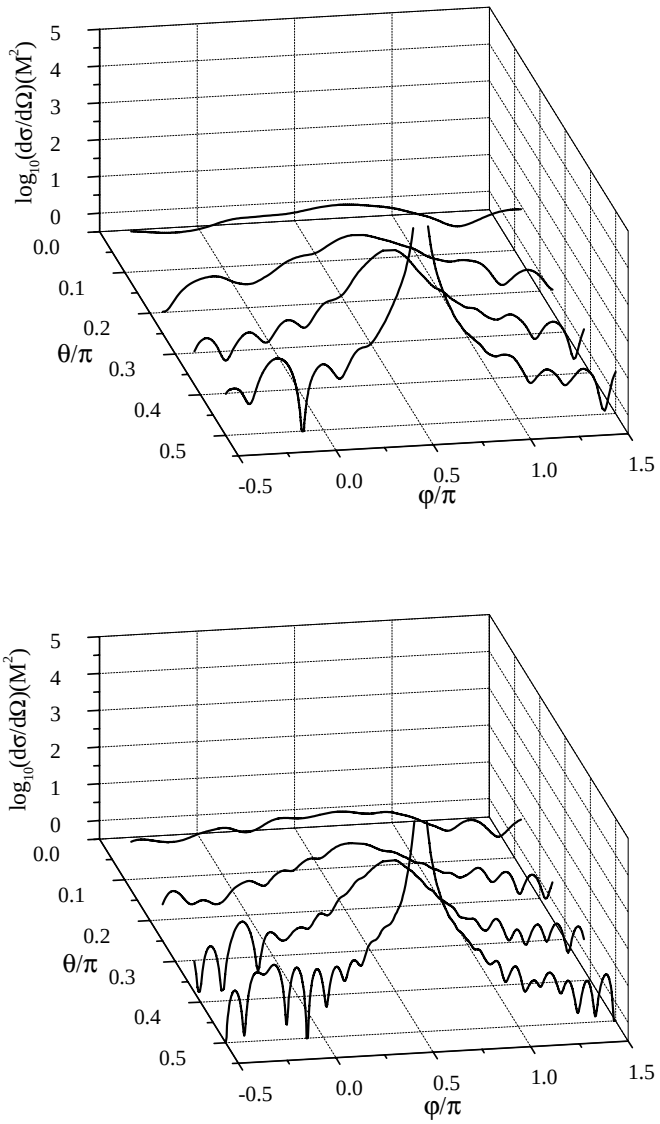

FIG. 9. Off-axis cross sections ($\theta = \pi/8, \pi/4, 3\pi/8, \pi/2$) for a black hole with spin $a = 0.9M$ and scattered waves with frequency $\omega M = 1$ (upper panel) and $\omega M = 2$ (lower panel). The incident wave is travelling in the $(\theta, \varphi) = (\pi/2, \pi/2)$ direction.

In order to understand the features seen in Fig. 9 further, we focus on the $\theta = \pi/2$ cross section. In Fig. 10 we show these "equatorial" cross sections for a sequence of spin rates $a/M = 0.2, 0.5, 0.7, 0.9$. As before, we have considered two different wave frequencies, $\omega M = 1$ and $\omega M = 2$. From the results shown in Fig. 10 it is clear that that the glory maximum is typically not observed in the backward ($\varphi = -\pi/2$) direction. In fact, it is clear that the maximum of the glory oscillations move away from the backward direction as the spin of the black hole is increased. A similar shift is seen in all interference oscillations. This behaviour is easy to explain in terms of the anticipated rotational frame-dragging. In order to illustrate this argument, we consider the geometric optics limit where partial waves are represented by null rays. Recall that in axisymmetric scattering the backward glory is associated with the divergence of the classical cross section at $\Theta = \pi$ in such a way that

$$\left(\frac{d\sigma}{d\Omega}\right)_{\rm cl} = \frac{b}{\sin\Theta}\left(\frac{d\Theta}{db}\right)^{-1} \tag{51}$$

The divergence is a result of the intersection of an infinite number of rays. For simplicity, let us consider rays travelling in a specified plane. Scattering near the backward direction by a Schwarzschild black hole is illustrated in Fig. 11

(left panel). Two rays with different impact parameters emerge at any given angle. These two waves make the main contribution to cross section at that particular angle. It is clear that for scattering at $\theta = \pi$ the two rays in Fig. 11 will follow symmetric trajectories. This means that when observed at infinity, after being scattered, the two waves will have equal phases (provided their initial phases were equal). In effect, these two rays will then constructively interfere in the exact backward direction. As we move away from the backward direction, we should observe a series of interference maxima and minima — the two rays will now have an overall phase difference since they follow different orbits (see Fig. 11). A very crude estimate of the location of the successive maxima would be $\theta_{\rm n} \sim n\pi/3\omega M$ where $n = 0, 1, 2, ...$, in reasonable agreement with the exact results.

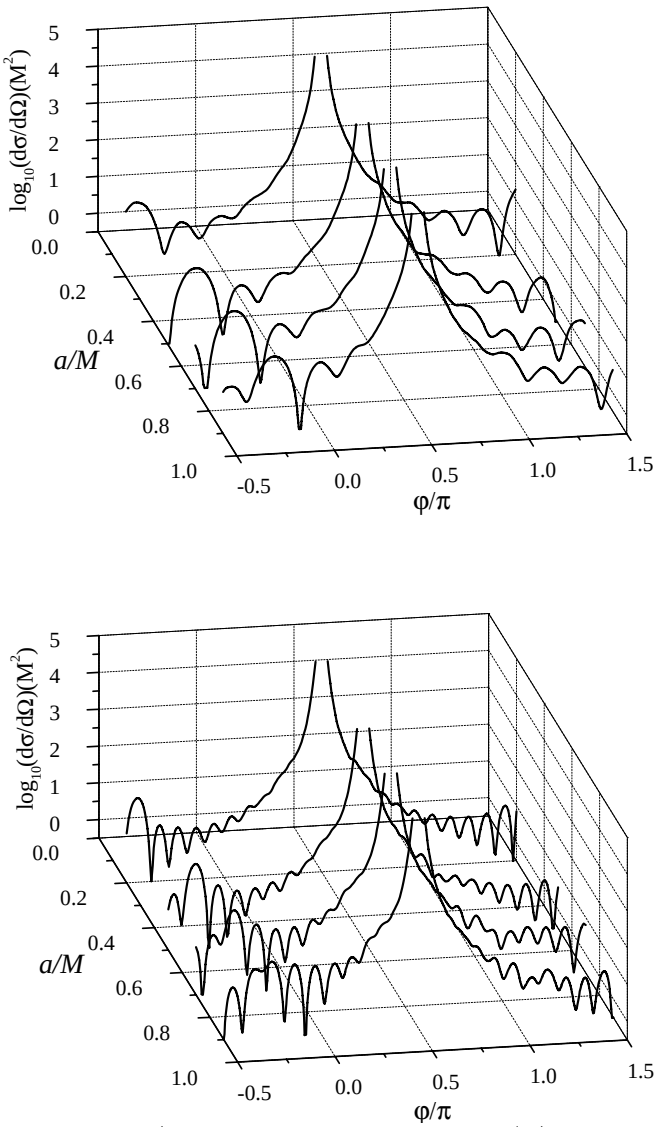

FIG. 10. Off-axis cross sections for $\theta = \pi/2$ and various black-hole spins (a/M= 0.2, 0.5, 0.7, 0.9) and scattered wave frequencies $\omega M = 1$ (upper panel) and $\omega M = 2$ (lower panel).

Similar arguments apply in the case of a Kerr black hole. We shall consider only equatorial rays, cf. Fig 11 (right panel). As a result of the discrimination between prograde and retrograde orbits, the two rays contributing to the cross section in the exact backward direction will no longer follow symmetric paths. In fact, the ray symmetric to the prograde ray shown in Fig 11 will follow a plunging orbit. Therefore, we should not expect the interference maximum to be located in the exact backward direction. An estimate (based on a crude calculation of the phase difference between the two null rays) of the location of the main backward glory maximum yields

$$\varphi_{\rm max} \sim \pi \left(\frac{r_{\rm ph+} - r_{\rm ph-}}{r_{\rm ph+} + r_{\rm ph-}} \right) \tag{52}$$

where $r_{\rm ph+}$ and $r_{\rm ph-}$ denote, respectively, the location of the prograde and retrograde unstable photon orbits (in Boyer-Lindquist coordinates). This angle is measured from the backward direction in the direction of the black hole's rotation. This simple prediction agrees reasonably well with the results inferred from our numerical cross sections. In a similar way, all other maxima and minima will be frame-dragged in the black hole's rotational direction.

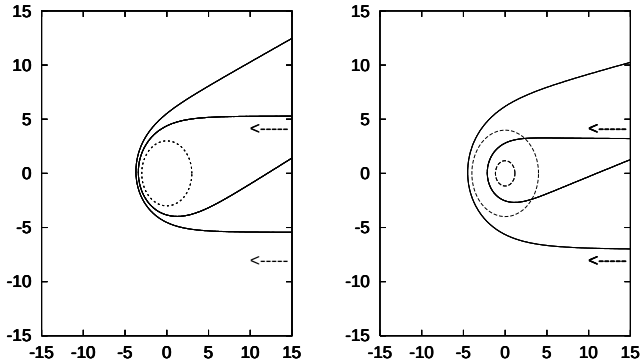

FIG. 11. Equatorial null geodesics (viewed from "above") around a Schwarzschild (left panel) and Kerr black hole (right panel). The figures are scaled in units of M. The rays are assumed to arrive from infinity (they enter from the right side of each figure in the direction indicated by the arrows) in parallel directions and exit at the same angle after being scattered. The dashed circles represent the unstable photon circular orbits. The Kerr black hole, in the right panel, is taken to rotate counter-clockwise with $a = 0.99M$.

To complete this discussion we consider the deflection function $\Phi(l, m)$ for "equatorial" partial waves ($m = \pm l$), an $a = 0.9M$ black hole and $\omega M = 1$. The corresponding data is shown in Fig. 12. There are two distinct logarithmic divergences which are associated with the existence of separate unstable circular photon orbits for prograde and retrograde motion. Note that for $m > 0$ the deflection function diverges steeper than it does for $m < 0$. The origin of this effect is the fact that prograde partial waves with $b \sim b_{\rm c}$ perform a greater number of revolutions (before escaping to infinity) than retrograde ones. Finally, for $|m| \gg 1$ we recover, as expected, the Einstein deflection angle $\Phi \approx -4M/b$ (not explicitly shown in the figure).

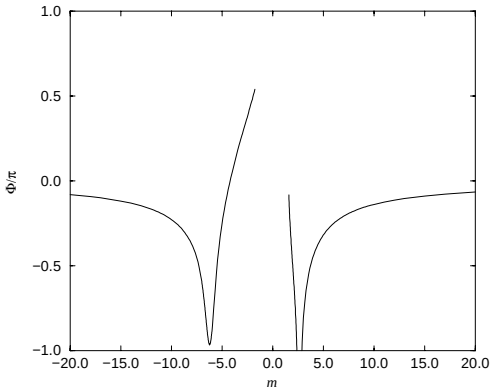

FIG. 12. The deflection function Φ for off-axis scattering is shown as a function of m for "equatorial" partial waves $m = \pm l$. The black hole spin is $a = 0.9M$ and the wave frequency is $\omega M = 1$. The small $|m|$ region is not included because of the inaccuracies discussed in Section IIIA.

E. Digression: forward glories

The results presented in the preceeding sections clearly show that, in general, black hole cross sections are dominated by a "Coulomb divergence" in the forward direction and (frame-dragged) glory oscillations near the backward direction.

However, according to the predictions of geometrical optics [1], one would expect to find glory oscillations also in the forward direction (see comments in [8]). For the case of Schwarzschild scattering, this effect would be associated with partial waves scattered at angles $\Theta = 0, -2\pi, -4\pi, ...$ Inspection of the relevant deflection function (Fig. 6) indicates that a partial wave which has $\Theta = 0$ will also be strongly absorbed, since it has an impact parameter $b < b_c$. Hence, we would expect its contribution to the forward glory to be severely supressed. It thus follows that, as far as the possible forward glory is concerned, the most important partial waves are those with $\Theta = -2\pi$. These partial waves "whirl" around the black hole as they have $b \approx b_c$.

Ford and Wheeler's semiclassical approach [25] shows that the forward glory is well approximated (for $\theta \approx 0$) by (50), although with a slightly different proportionality factor. However, we should obviously not expect to see a pronounced forward glory in the cross section, as it will drown in the forward Coulomb divergence. Still, as an experiment aimed at supporting our intuition, we can try to "dig out" the forward glory pattern. This has to be done in a somewhat artificial manner, but since the forward glory is due to scattering and interference of partial waves with $b \approx b_c$ we can isolate their contribution by truncating the sum in f_D at some $l_{\rm max} \sim \omega b_c$ and at the same time neglecting the Newtonian part f_N entirely. It is, of course, important to realize that this "truncated" cross section is not a physical (observable) quantity.

In Fig. 13 we show the result of this "truncated cross section" calculation for the case of a Schwarzschild black hole and $\omega M = 2$. We compare results for two levels of truncation, $l_{\rm max} = 10$ and 15. In the first case, a clear Bessel- function like behaviour arises (it is straightforward to fit a $J_0^2(\omega b_c \sin\theta)$ function to the solid curve in Fig. 13). This confirms our expectation that there is, indeed, a forward glory present in the data. As more partial waves are included the cross section begins to deviate from the glory behaviour, and if we increase $l_{\rm max}$ further the forward glory is swamped by terms that contribute to the Coulomb divergence.

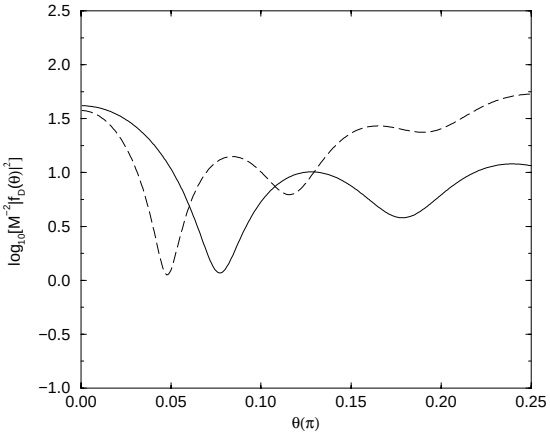

FIG. 13. Illustration of a forward glory in Schwarzschild scattering. The "diffraction" piece $|f_D(\theta)|^2$ of the cross section is shown in the vicinity of the forward direction, for wave frequency $\omega M = 2$ and for $l_{\rm max} = 10$ (solid curve) and $l_{\rm max} = 15$ (dashed curve).

F. The role of superradiance in the scattering of monochromatic waves.

Superradiance is an interesting effect known to be relevant for rotating black holes. It is easily understood from the asymptotic behaviour (6) of the causal solution to the scalar-field Teukolsky equation (4). If we use this solution and its complex conjugate, and the fact that two linearly independent solutions to (4) must lead to a constant Wronskian, it is not difficult to show that

$$(1 - m\omega_+/\omega)|\mathcal{T}_{lm}|^2 = 1 - |\mathcal{S}_{lm}|^2 \ . \tag{53}$$

where we have defined

$$|\mathcal{T}_{lm}|^2 = \left|\frac{1}{A^{\rm in}_{lm}}\right|^2 \ . \tag{54}$$

From the above result it is evident that the scattered waves are amplified ($|\mathcal{S}_{lm}|^2 > 1$) if $\omega < m\,\omega_+$. This amplification is known as superradiance.

In principle, one would expect superradiance to play an important role in the scattering problem for rapidly spinning black holes. For example, one could imagine that some partial waves which would otherwise be absorbed, could escape back to infinity. These waves might then possibly make a noticeable contribution to the diffraction cross section, provided that there were a sufficient number of them (as compared to the total number $l_{\rm max}$ of partial waves contributing to the diffraction scattering amplitude).

In order to investigate this possibility, we have performed a number of off-axis cross section calculations for a variety of wave frequencies $\omega M = 0.5 - 10$ and for $a \approx M$, i.e. black holes spinning near the extreme Kerr limit. We have found no qualitive difference whatsoever between those cross-sections and the ones for a somewhat smaller spin value, $a = 0.9M$ (say). In essence, we were unable to find any effects in the cross section that could be attributed to superradiance. Consequently, we are led to suspect that our intuition regarding the importance of superradiance for the scattering problem may be wrong.

This suspicion is confirmed by the following simple argument. In order for a partial wave to be superradiant we should have $0 < \omega < m\omega_+$. Considering an extreme Kerr black hole (which provides the best case for superradiant scattering) and the fact that $m \leq l$, we have the condition

$$0 < 2\omega M < l \tag{55}$$

As already mentioned, the partial waves for which superradiance will be important are the ones with impact parameters $b \lesssim b_{\rm c}$, i.e. those that would be absorbed under different circumstances. This then requires that

$$l \lesssim \omega b_{\rm c} - 1/2 \tag{56}$$

Combining (55) and (56) we arrive at the inequality

$$0 < 2M \lesssim b_{\rm c} - 1/2\omega \tag{57}$$

The critical impact parameter (for prograde motion) for an $a = M$ black hole is $b_{\rm c} \approx 2M$. Hence the condition (57) will not be satisfied, and it is unlikely that we would get a significant number of (if any) superradiant partial waves that could affect the cross section.

This conclusion may seem surprising given results present in the literature [1,9]. In particular, Handler and Matzner have briefly discussed the effect of superradiance on axially incident gravitational waves. They argue that (see figure 14 in [9]) "superradiance has the effect of imposing a large background over the pattern, filling in the interference minima". Given our current level of understanding (or lack thereof) we cannot at this point say whether superradiance can be the explanation for the effects observed by Handler and Matzner. After all, one should remember that superradiant scattering strongly depends on the spin of the field that is being scattered. It is well known [22] that gravitational perturbations can be amplified up to 138% compared to a tiny 0.04% amplification for scalar fields (which is the case considered in this paper). This means that superradiance may significantly affect also partial waves with $b > b_{\rm c}$ in the gravitational wave case, which could lead to our simple argument not being valid. This issue should be addressed by a detailed study of the scattering of gravitational waves from rotating black holes.

IV. CONCLUDING DISCUSSION

We have presented an investigation of scattering of massless scalar waves by a Kerr black hole. Our numerical work is based on phase-shifts obtained via integration of the relevant radial wavefunction with the help of the Prüfer phase-function method. This method has been shown to be computationally efficient and to provide accurate results. Using the obtained phase-shifts we have constructed differential cross sections for several different cases. First we have discussed the case of waves incident along the black hole's rotation axis, for which we showed that the resulting cross sections are similar to ones obtained in the (non-rotating) Schwarzschild case. We then turned to the case of off-axis incidence, where the situation was shown to change considerably. In that case the cross sections are generically asymmetric with respect to the incidence direction. The overall diffraction pattern is "frame dragged", and as a result the backward glory maximum is shifted along with of the black hole's rotation. Moreover, we have concluded that (at least for scalar waves) the so-called superradiance effect is unimportant for monochromatic scalar wave scattering.

To summarize, our study provides a complete understanding of the purely rotational effects involved in black-hole scattering. Given this we are now well equipped to proceed to problems of greater astrophysical interest, particularly ones concerning gravitational waves. In these problems one would expect further features to arise as the spin and polarisation of the impinging waves interact with the spin of the black hole. For incidence along the hole's spin axis,

one can have circularly polarised waves which are either co- or counter-rotating. The two cases can lead to quite different results. Although the general features of the corresponding cross sections are similar, they show different structure in the backward direction [1]. This is possibly due to interference between the two polarisation states of gravitational waves, an effect that has not yet been explored in detail. Some initial work on gravitational-wave scattering has been done, see [9], but we believe that the results of the present paper sheds new light on previous results, and could help interpret the rather complex cross sections that have been calculated in the gravitational-wave case.

In this context, it should be stressed that the choice of studying scalar waves was made solely on grounds of clarity and simplicity. Our approach can readily be extended to other cases. Moreover, it is relevant to point out that a full off-axis gravitational wave scattering cross section calculation is still missing. We would expect such cross sections to be rather complicated, combining the frame-dragging effects discussed in this paper with various spin-induced features. We hope to be able to study this interesting problem in the near future.

ACKNOWLEDGMENTS

K.G. thanks the State Scholarships Foundation of Greece for financial support. N.A. is a Philip Leverhulme Prize Fellow, and also acknowledges support from PPARC via grant number PPA/G/1998/00606 and the European Union via the network "Sources for Gravitational Waves".

APPENDIX A: PLANE WAVES IN THE KERR GEOMETRY

The long-range character of the gravitational field modifies the form of "plane waves". This non-trivial issue has been discussed in the context of black hole scattering by Matzner [23] and Chrzanowski *et al.* [24]. For completeness, we provide a brief discussion here.

In a field-free region a monochromatic plane wave is, of course, given by the familiar expression

$$\Phi_{\rm plane} = e^{i\omega r\cos\theta - i\omega t} \tag{A1}$$

when a spherical coordinate frame is employed. The plane wave is taken to travel along the z-axis. The field in (A1) solves the the wave equation $\Box\Phi_{\rm plane} = 0$. Moreover, we can assume a decomposition of the form

$$\Phi_{\rm plane} = \frac{e^{-i\omega t}}{r}\sum_l c_l^{(0)} u_l^{(0)}(r) P_l(\cos\theta) e^{-i\omega t} \tag{A2}$$

where the radial wavefunction satisfies

$$\frac{d^2u_l^{(0)}}{dr^2} + \left[\omega^2 - \frac{l(l+1)}{r^2}\right] u_l^{(0)} = 0 \tag{A3}$$

Let us now consider a "plane wave" in the Schwarzschild geometry. First of all, we expect such a field to be only an asymptotic solution (as $r\to\infty$) of the full wave equation $\Box\Phi = 0$ (where $\Box$ represents the covariant d'Alembert operator). The plane wave field can then be represented at infinity as

$$\Phi_{\rm plane} \approx \frac{e^{-i\omega t}}{r}\sum_l c_l^{(0)} u_l^{(0)}(r) P_l(\cos\theta) e^{-i\omega t} \tag{A4}$$

and the radial wavefunction will be a solution of

$$\frac{d^2u_l^{(0)}}{dr_*^2} + \left[\omega^2 - \frac{l(l+1)}{r_*^2} + \mathcal{O}\left(\frac{\ln r_*}{r_*^3}\right)\right] u_l^{(0)} = 0 \tag{A5}$$

This equation is similar to the corresponding flat space equation. The only difference is the appearance of the tortoise coordinate r_* instead of r. Hence, we are inspired to write the plane wave field as

$$\Phi_{\rm plane} = e^{i\omega r_*\cos\theta - i\omega t} \tag{A6}$$

From this discussion, it should be clear that this form is valid only for $r \to \infty$. It is straightforward to see that in the same regime (A6) solves $\Box\Phi = 0$. Expression (A6) is the closest we can get to the usual plane wave form (A1). The long-range gravitational field is simply taken into account by an appropriate phase modification.

Next, we consider a plane wave in Kerr geometry. For simplicity we take the z-axis to coincide with the black hole's spin axis. We can then write

$$\Phi_{\rm plane} \approx \frac{e^{-i\omega t}}{r} \sum_l c_l^{(0)} u_l^{(0)}(r) S_{l0}^{a\omega}(\theta) e^{im\varphi} \tag{A7}$$

The radial wavefunction is solution of

$$\frac{d^2 u_l^{(0)}}{dr_*^2} + \left[\omega^2 - \frac{\lambda + 2am\omega}{r_*^2} + \mathcal{O}\left(\frac{\ln r_*}{r_*^3}\right)\right] u_l^{(0)} = 0 \tag{A8}$$

It is obvious that both (A7) and (A8) are different from the corresponding flat space expressions. That is, unlike in the Schwarzschild case, we are not able to derive an explicit form for a plane wave. Thus, we postulate the following asymptotic expression for a plane wave travelling along the z-axis

$$\Phi_{\rm plane} = e^{i\omega r_* \cos\theta - i\omega t} \tag{A9}$$

where r_* is the appropriate tortoise coordinate (5). The field given by (A9) is a solution of $\Box\Phi = 0$ for $r \to \infty$. For the general case of a plane wave travelling along a direction that makes an angle γ with the z-axis the appropriate expression is given by (8).

APPENDIX B: ASYMPTOTIC EXPANSION OF PLANE WAVES

In this Appendix the asymptotic expansion of a plane wave in Kerr background is worked out. The calculation presented here is identical to the one found in the Appendix A1 of [1], but here it is specialised to $s = 0$. We have seen that for $r \to \infty$ the plane wave decomposition becomes

$$e^{i\omega r_* [\sin\gamma \sin\theta \sin\varphi + \cos\gamma \cos\theta]} \approx \frac{1}{\omega r} \sum_{l,m} c_{lm}^{(0)} u_{lm}^{(0)}(r \to \infty) S_{lm}^{a\omega}(\theta) e^{im\varphi} \tag{B1}$$

where γ is the angle between the wave's propagation direction and the positive z-axis. We multiply this expression by $S_{l'm'}^{a\omega}(\theta') e^{-im'\varphi'}$ and integrate over the angles to get (after a trivial change $l' \to l$, $m' \to m$ at the end)

$$c_{lm}^{(0)} u_{lm}^{(0)}(r \to \infty) \approx \omega r \int_0^\pi d\theta \sin\theta \; S_{lm}^{a\omega}(\theta) e^{i\omega r_* \cos\gamma \cos\theta} \int_0^{2\pi} d\varphi e^{i\omega r_* \sin\gamma \sin\theta \sin\varphi - im\varphi} \tag{B2}$$

The integration over φ can be performed with a little help from [29], and the result is

$$\int_0^{2\pi} d\varphi e^{i\omega r_* \sin\gamma \sin\theta \sin\varphi - im\varphi} = 2\pi J_m(\omega r_* \sin\gamma \sin\theta) \tag{B3}$$

Since the Bessel function has a large argument it can be approximated as [28],

$$J_\nu(z) \approx \frac{1}{\sqrt{2\pi z}} \left(e^{i(z - \nu\pi/2 - \pi/4)} + e^{-i(z - \nu\pi/2 - \pi/4)}\right) \tag{B4}$$

Note that this approximation is legal as long as $\gamma \neq 0$. The on-axis case $\gamma = 0$ can be treated seperately, in a way similar to the one sketched here. Using this approximation in (B2) we get

$$c_{lm}^{(0)} u_{lm}^{(0)}(r \to \infty) \approx \sqrt{\frac{2\pi\omega r}{\sin\gamma}} \left(e^{-\frac{i}{2}(m\pi + \pi/2)} \mathcal{I}_- + e^{\frac{i}{2}(m\pi + \pi/2)} \mathcal{I}_+\right) \tag{B5}$$

$$\mathcal{I}_\pm = \int_0^\pi d\theta \sqrt{\sin\theta} S_{lm}^{a\omega}(\theta) e^{i\omega r_* \cos(\theta \pm \gamma)} \tag{B6}$$

The $\mathcal{I}_\pm$ integrals can be evaluated using the stationary phase approximation. We obtain

$$c_{lm}^{(0)} u_{lm}^{(0)}(r \to \infty) \approx 2\pi \left[(-i)^{m+1} e^{i\omega r_*} S_{lm}^{a\omega}(\gamma) + i^{m+1} e^{-i\omega r_*} S_{lm}^{a\omega}(\pi - \gamma)\right] \tag{B7}$$

We finally get (10) by using the symmetry relation

$$S_{lm}^{a\omega}(\pi - \theta) = (-1)^{l+m} S_{lm}^{a\omega}(\theta) \tag{B8}$$

APPENDIX C: CALCULATION OF SPHEROIDAL HARMONICS AND THEIR EIGENVALUES

For the numerical calculation of the spheroidal harmonics we have adopted a "spectral decomposition" method, first developed by Hughes [30] in the context of gravitational wave emission and radiation backreaction on particles orbiting rotating black holes. In the present work we have specialised this technique for the spin-0 spheroidal harmonics. The angular equation satisfied by $S^{a\omega}_{lm}(\theta)$ is,

$$\frac{1}{\sin\theta}\frac{d}{d\theta}\left(\sin\theta\frac{dS^{a\omega}_{lm}}{d\theta}\right)+[(a\omega)^2\cos^2\theta-\frac{m^2}{\sin^2\theta}+E_{lm}]S^{a\omega}_{lm}=0 \tag{C1}$$

where E_{lm} denotes the corresponding eigenvalue. For the special case $a\omega=0$ we have $E_{lm}=l(l+1)$ and the solution of (C1) is the familiar spherical harmonic (here we are suppressing the dependence on φ)

$$Y_{lm}(\theta)=\left[\frac{2l+1}{4\pi}\frac{(l-m)!}{(l+m)!}\right]^{1/2}P_{lm}(\cos\theta) \tag{C2}$$

where P_{lm} is the associated Legendre polynomial. It's numerical calculation is quite straigthforward [27] based on the recurrence relation

$$P_{lm}(x)=\frac{1}{l-m}[x(2l-1)P_{l-1,m}-(l+m-1)P_{l-2,m}] \tag{C3}$$

with "initial conditions"

$$P_{mm}(x)=(-1)^m(2m-1)!!(1-x^2)^{m/2} \tag{C4}$$
$$P_{m+1,m}(x)=(2m+1)xP_{mm}(x) \tag{C5}$$

We can always expand the spheroidal harmonic in terms of spherical harmonics,

$$S^{a\omega}_{lm}(\theta)=\sum_{j=|m|}^{\infty}b^{a\omega}_j Y_{jm}(\theta) \tag{C6}$$

Substituting this spectral decomposition in (C1), multiplying with $Y_{lm}(\theta)$ and integrating over θ we get

$$(a\omega)^2\sum_{j=|m|}^{\infty}b^{a\omega}_j c^m_{jl2}-b^{a\omega}_l l(l+1)=-E_{lm}b^{a\omega}_l \tag{C7}$$

where

$$c^m_{jl}=2\pi\int_0^{\pi}d\theta\sin\theta\cos^2\theta\ Y_{lm}(\theta)Y_{jm}(\theta) \tag{C8}$$

This integral can be evaluated in terms of Clebsch-Gordan coefficients [28]

$$c^m_{jl}=\frac{1}{3}\delta_{lj}+\frac{2}{3}\sqrt{\frac{2j+1}{2l+1}}<j2m0|lm><j200|l0> \tag{C9}$$

It follows that $c^m_{jl}\neq 0$ only for $j=l-1,l,l+1$. Then (C7) gives

$$[(a\omega)^2c^m_{l-2,l}]b^{a\omega}_{l-2}+[(a\omega)^2c^m_{l,l}-l(l+1)]b^{a\omega}_l+[(a\omega)^2c^m_{l+2,l}]b^{a\omega}_{l+2}=-E_{lm}b^{a\omega}_l \tag{C10}$$

We can rewrite (C10) as an eigenvalue problem for the matrix $M_{ij}=(a\omega)^2c^m_{ji}$ with eigenvector $b^i=b^{a\omega}_i$ and eigenvalue E_{lm}. Clearly, $\mathbf{M}$ is a real band-diagonal matrix. Standard routines from [27] can be employed to find the eigenvectors and eigenvalues of such a matrix. Then, the spheroidal harmonic is directly obtained from (C6) (even though it involves an infinite sum, in reality only few coefficients $b^{a\omega}_j$ are significant). The described spectral decomposition method is reliable, unless $a\omega$ becomes large compared to unity (under such conditions the matrix $\mathbf{M}$ is no longer diagonally dominant, and the convergence of the method is very slow). In effect, very high frequency cross sections for Kerr scattering will be inaccurate (especially when the black hole is rapidly rotating).

[1] J.A.H. Futterman, F.A. Handler and R.A. Matzner, *Scattering from Black Holes* (Cambridge University Press, Cambridge, England, 1988).
[2] R.A. Matzner and M.P. Ryan, Jr., Astrophys. J. Suppl. **36**, 451 (1978).
[3] N. Sanchez, J. Math. Phys. **17**, 688 (1976)
[4] N. Sanchez, Phys. Rev. D **16**, 937 (1977)
[5] N. Sanchez, Phys. Rev. D **18**, 1030 (1978)
[6] N. Sanchez, Phys. Rev. D **18**, 1798 (1978)
[7] P. Anninos, C. DeWitt-Morette, R.A. Matzner, P. Yioutas, and T-R Zhang, Phys. Rev. D **46**, 4477 (1992)
[8] N. Andersson, Phys. Rev. D **52**, 1808 (1995)
[9] F.A. Handler and R.A. Matzner, Phys. Rev. D **22**, 2331 (1980)
[10] R.G. Newton, *Scattering Theory of Waves and Particles* (McGraw-Hill, New York, 1966).
[11] N. Andersson and K-E. Thylwe, Class. Quantum Grav. **11**, 2991 (1994)
[12] N.Andersson, Class. Quantum Grav. **11**, 3003 (1994)
[13] C. DeWitt-Morette and B.L. Nelson, Phys. Rev. D **29**, 1663 (1984)
[14] T-R Zhang and C. DeWitt-Morette, Phys. Rev. Lett. **52**, 2313 (1984)
[15] N. Fröman, P.O. Fröman, and B. Lundborg, Math. Proc. Cambridge Philos. Soc. **104**, 153 (1988)
[16] N. Fröman, P.O. Fröman, in *Forty More Years of Ramifications: Spectral Asymptotics and its Applications*, edited by S.A. Fulling and F.J.Narcowich, Discourses in Mathematics and its Applications, No. 1(Texas A& M University, Department of Mathematics, 1992), pp 121-159
[17] P. Pajunen, J. Chem. Phys. **88**, 4268, (1988)
[18] P. Pajunen, J. Comp. Phys. **82**, 16, (1989)
[19] J.D. Pryce, *Numerical Solution of Sturm-Liouville Problems* (Oxford Science Publications, Oxford, England, 1993)
[20] N. Andersson, Proc. R. Soc. Lon. A **439**, 47, (1992)
[21] S.A. Teukolsky, Astrophys. J. **185**, 635 (1973)
[22] S.A. Teukolsky and W.H. Press, Astrophys. J. **193**, 443 (1974)
[23] R.A. Matzner, J.Math.Phys. **9**, 163 (1968)
[24] P.L. Chrzanowski, R.A. Matzner, V.D. Sandberg, and M.P. Ryan, Jr. , Phys. Rev. D **14**, 317 (1976)
[25] K.W. Ford and J.A. Wheeler, Ann. Phys. (N.Y.) **7**, 287 (1959)
[26] S. Chandrasekhar, *The Mathematical Theory of Black Holes* (Oxford University Press, New York, 1983)
[27] W.H. Press, S.A. Teukolsky, W.T. Vetterling and B.P. Flannery, *Numerical Recipes* (Cambridge University Press, Cambridge, England, 1992).
[28] M. Abramowitz and I.A. Stegun *Handbook of Mathematical Functions* (Dover Publications INC., New York, 1985)
[29] I.S. Gradshteyn and I.M. Ryzhik, *Tables of Integrals, Series and products* (Academic Press INC., London 1980)
[30] S.A. Hughes, Phys. Rev. D **61**, 084004 (2000)